Identification of microtearing modes below the ion gyroscale in the National Spherical Torus Experiment

2011 Plasma Phys. Control. Fusion 53 035013

(http://iopscience.iop.org/0741-3335/53/3/035013)

IOP PUBLISHING PLASMA PHYSICS AND CONTROLLED FUSION

Plasma Phys. Control. Fusion **53** (2011) 035013 (9pp) doi:10.1088/0741-3335/53/3/035013

Identification of microtearing modes below the ion gyroscale in the National Spherical Torus Experiment

D R Smith[1], W Guttenfelder[2], B P LeBlanc[2] and D R Mikkelsen[2]

[1] Department of Engineering Physics, University of Wisconsin-Madison, Madison, WI 53706, USA
[2] Princeton Plasma Physics Laboratory, Princeton, NJ 08543, USA

E-mail: drsmith@engr.wisc.edu

Received 9 October 2010, in final form 22 December 2010
Published 28 January 2011
Online at stacks.iop.org/PPCF/53/035013

Abstract

Gyrokinetic calculations indicate microtearing modes below the ion gyroscale are linearly unstable in a National Spherical Torus Experiment (NSTX) plasma. The modes are robustly unstable with respect to simulation parameters, radial location and discharge time. The modes exist at higher wavenumbers and exhibit narrower electric potential mode structures than conventional microtearing modes, but both modes extend to similar normalized radial wavenumbers. Mode growth rates increase with higher electron temperature gradients and higher collisionality. Finally, microtearing modes below the ion gyroscale are the most unstable modes near the magnetic axis, but electron temperature gradient modes are the most unstable modes in the outer plasma region.

(Some figures in this article are in colour only in the electronic version)

1. Introduction

The microtearing mode is a small-scale magnetic island destabilized by current at the island boundary [1–6]. When island chains at nearby rational surfaces grow sufficiently large and overlap, a stochastic magnetic field region with enhanced electron thermal transport develops. Microtearing instabilities may contribute to the anomalous electron thermal transport observed in spherical torus (ST) and tokamak plasmas, but gyrokinetic calculations indicate microtearing instabilities can be more virulent in ST plasmas due to flow shear suppression of drift-wave turbulence [1–3]. National Spherical Torus Experiment (NSTX) [7–9] plasmas with sufficient neutral beam heating exhibit neoclassical ion thermal and particle transport, but electron thermal transport remains anomalous and the dominant transport mechanism [10–12]. Recent linear gyrokinetic calculations and scaling relations indicate conventional microtearing

instabilities may account for the electron thermal transport inferred in NSTX beam-heated H-mode plasmas [11, 13–17].

The electron temperature gradient provides free energy to drive microtearing instabilities [18]. Proposed drive mechanisms for microtearing instabilities include the parallel thermal force in collisional plasmas [19, 20] and electron scattering at the trapped-passing boundary in low collisionality plasmas [21, 22]. In the collisionless limit, the microtearing mode is stable [23]. In addition, recent gyrokinetic calculations indicate magnetic drifts among passing electrons provide another drive mechanism with an energy-independent collision operator [1]. All proposed drive mechanisms generate the destabilizing current at magnetic island boundaries. Microtearing modes are fundamentally electromagnetic with even parity parallel vector potential perturbations ($\tilde{A}_\parallel$) and odd parity electric potential perturbations ($\tilde{\Phi}$). In contrast, drift-wave modes, such as the ion temperature gradient mode, are largely electrostatic with even parity $\tilde{\Phi}$, though electromagnetic effects can impact drift-wave dynamics [24].

Prior investigations of microtearing instabilities were limited to modes with $k_y\rho_s \leqslant 1$ where ρ_s is the ion sound radius and k_y is the binormal wavenumber. The binormal direction is the direction perpendicular to the magnetic field in a flux surface. Here, we investigate microtearing modes below the ion gyroscale ('high-k') with `GS2` linear gyrokinetic simulations [25–27]. Section 2 describes linearly unstable high-k microtearing modes with $3 < k_y\rho_s < 15$ in a NSTX L-mode plasma. The modes are robustly unstable, and the calculations are converged with respect to simulation parameters, such as time step. Compared with conventional microtearing modes, the $\tilde{\Phi}$ mode structures are narrower in ballooning angle. Section 3 illustrates growth rate dependences with parameters scans in gradients, equilibrium parameters and collisionality. Section 4 investigates the existence of additional microinstabilities across the plasma profile. Notably, high-k microtearing instabilities are dominant near the magnetic axis, but electron temperature gradient instabilities are dominant in the outer plasma. Finally, section 5 summarizes results.

2. Identification of microtearing modes below the ion gyroscale

Figure 1 shows plasma parameters for a NSTX helium L-mode discharge with 600 kA of plasma current and 1.2 MW of high-harmonic fast-wave heating [28, 29]. The Mirnov signal indicates the plasma is MHD quiescent during times of interest. Plasma parameters for gyrokinetic simulations are derived from multi-point Thomson scattering measurements [30, 31] and `EFIT` equilibrium reconstructions. Ion temperature measurements from charge-exchange spectroscopy are not available due to the absence of neutral beam heating, but neutral beam 'blips' in similar discharges indicate the ion temperature profile is broad with peak $T_i \approx 1$ keV. Accordingly, ion temperature parameters in the following gyrokinetic simulations are set to $T_i = \min\{0.85 \times T_e, 1\,\text{keV}\}$ and $a/L_{T_i} = a/L_{T_e} \times (T_i/T_e)$ where $a/L_X \equiv (1/X)(\mathrm{d}X/\mathrm{d}\rho)$, a is the last closed flux surface half-width, $\rho \equiv r/a$ and r is the flux surface half-width.

Plasma parameters derived from figure 1 and listed in table 1 were analyzed for microinstabilities using `GS2`, an initial-value, electromagnetic, continuum gyrokinetic code [25–27]. The gyrokinetic model is valid for modes with arbitrary $k_\perp\rho_s$ including high-k modes with $k_\perp\rho_s \gg 1$ [25]. For linear calculations, `GS2` evolves the gyrokinetic equations to obtain frequency, growth rate and mode structures of the fastest growing mode at specified k_y. Figure 2 shows $\tilde{\Phi}$ and $\tilde{A}_\parallel$ mode structures and growth rates for plasma parameters in figure 1 and table 1. Each simulation includes eight modes in the range $k_y\rho_s = 3$–15, and only converged microtearing modes (odd parity $\tilde{\Phi}$ and even parity $\tilde{A}_\parallel$) are retained for analysis. The high-k

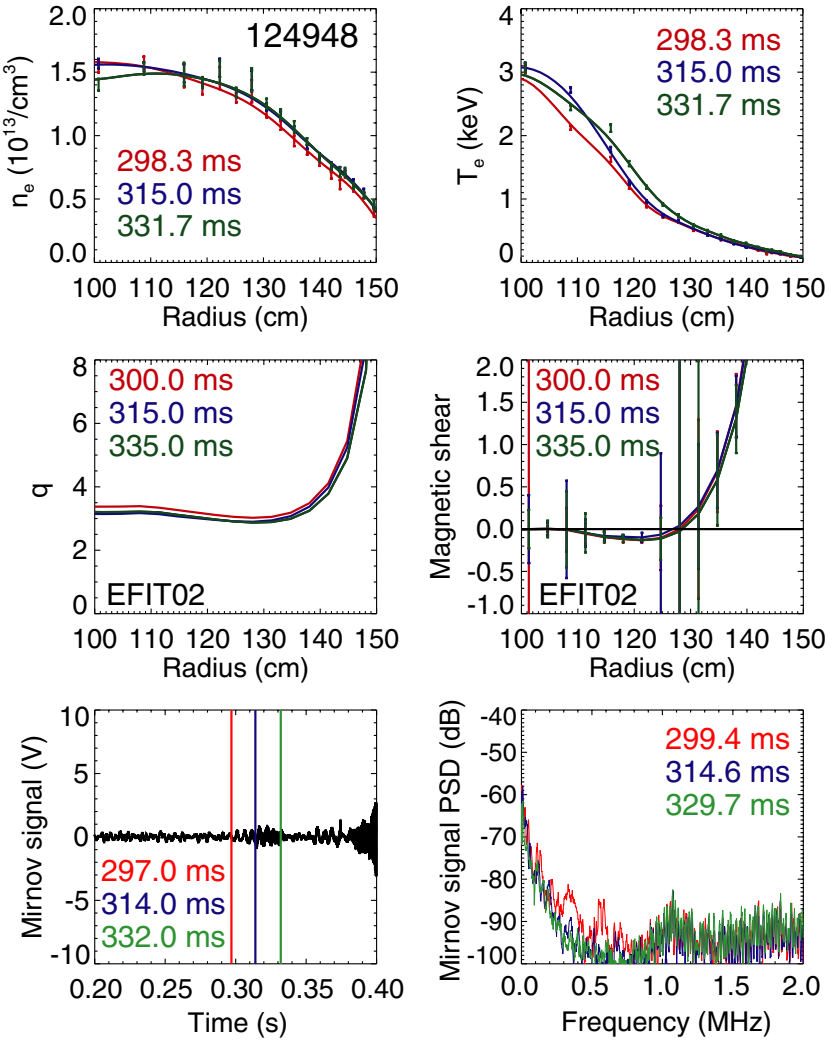

Figure 1. Profile quantities and Mirnov signal for the NSTX helium L-mode discharge 124948.

microtearing modes are linearly unstable in an extended radial region. Fully and partially electromagnetic simulations produce nearly identical growth rates, but the modes fail to grow above residual noise in electrostatic simulations. Accordingly, the modes are fundamentally electromagnetic.

The high-k microtearing modes in figure 2 are converged with respect to simulation parameters and persist for multiple time periods. Figure 3 shows growth rate radial profiles for different simulation parameters and at multiple discharge times. The growth rates in figure 3 represent the maximum growth rate among converged microtearing modes in the range $3 < k_y\rho_s < 15$ at each radii. In baseline simulations, the time step is $\Delta t/(a/v_t) = 0.014$, the θ domain is $|\theta| \leqslant 13 \times 180^\circ$ with resolution $\Delta\theta = 180^\circ/16$, and the energy domain is $E/(k_B T_e) = 0$–6 with 14 energy grid points. The simulations are converged with respect to time step, θ domain, θ grid resolution and energy grid resolution. In addition, growth rate profiles at 298 and 330 ms are similar to growth rate profiles at 315 ms. The numerical

Table 1. Plasma parameters for figure 1 at 315 ms. R is the major radius, R_{gs} is the flux surface geometric center and r is the flux surface half-width. The last closed flux surface half-width and geometric center are $a = 65.9$ cm and $R_0 = 85.6$ cm, respectively, and the magnetic field is 5.63 kG at R_0.

R (cm)	110	115	121	130
R_{gc} (cm)	100.9	100.3	99.3	97.2
r (cm)	9.1	14.7	21.7	32.8
$\epsilon \equiv r/R_{gc}$	0.09	0.14	0.22	0.34
$\rho \equiv r/a$	0.14	0.22	0.33	0.50
dR_{gc}/dr	−0.11	−0.10	−0.17	−0.22
q (safety factor)	3.47	3.34	3.18	3.04
$\hat{s} \equiv (r/q)(dq/dr)$	−0.04	−0.11	−0.15	0.06
κ (elongation)	1.97	1.98	1.99	2.01
$d\kappa/d\rho$	0.11	0.10	0.10	0.10
δ (triangularity)	0.08	0.12	0.18	0.27
$d\delta/d\rho$	0.55	0.55	0.55	0.55
n_e (10^{13} cm^{-3})	1.54	1.50	1.43	1.24
a/L_{n_e}	0.23	0.38	0.53	1.27
T_e (keV)	2.49	1.85	1.10	0.56
a/L_{T_e}	2.62	4.34	5.07	3.61
T_i (keV)	1.00	1.00	0.94	0.47
a/L_{T_i}	1.05	2.34	4.31	3.07

convergence, radial extent and temporal persistence of high-k microtearing modes in figure 3 indicate the modes are robustly unstable.

The mode structures in figure 2 are plotted as a function of ballooning angle θ which marks the distance along magnetic field lines using the poloidal angle [1]. Compared with conventional microtearing modes, the high-k microtearing modes exhibit narrower $\tilde{\Phi}$ mode structures and broader $\tilde{A}_\parallel$ mode structures. Specifically, high-k microtearing modes exhibit $\tilde{\Phi}$ mode structures that extend to $\theta \approx \pm 8 \times 180^\circ$ and $\tilde{A}_\parallel$ mode structures that extend to $\theta \approx \pm 5 \times 180^\circ$. Mode structures can be transformed into radial wavenumber (k_r) spectra using the relation

$$k_r = \hat{s} k_\theta (\theta - \theta_0) \tag{1}$$

where $\hat{s}$ is the magnetic shear [24]. The modes in figure 2 exist near the magnetic axis where the magnetic shear is low with $\hat{s} \approx -0.1$, so $|\hat{s}| \times k_\theta \rho_s \approx 1$ and $k_r \rho_s$ spectra extend to approximately $\pm 8\pi$ and $\pm 5\pi$ for $\tilde{\Phi}$ and $\tilde{A}_\parallel$, respectively. On the other hand, conventional microtearing modes in [1, 2] exhibit $\tilde{\Phi}$ mode structures that extend to $\theta \approx \pm 30 \times 180^\circ$ and $\tilde{A}_\parallel$ mode structures that extend to $\theta \approx \pm 180^\circ$. Conventional microtearing modes exhibit $\hat{s} \times k_\theta \rho_s \approx 0.5$, so $k_r \rho_s$ spectra extend to approximately $\pm 15\pi$ and $\pm \pi/2$ for $\tilde{\Phi}$ and $\tilde{A}_\parallel$, respectively. It is notable that $k_r \rho_s$ spectra for both high-k and conventional microtearing modes extend to similar $k_r \rho_s$ values for $\tilde{\Phi}$, namely about $\pm 10\pi$. The similar $k_r \rho_s$ ranges suggest high-k microtearing mode may require a radial resolution similar to conventional microtearing modes to resolve the narrow current layer. In turn, the radial resolution may determine the extent of eigenfunctions in ballooning angle via equation (1).

High-k and conventional microtearing modes also exist at similar toroidal and poloidal mode numbers, n and m, respectively. Mode numbers are given by $k_\theta = nq/r$ and $m = nq$ where r is the minor radius and q is the safety factor. The modes in figure 2 exist at $k_\theta \approx 10\,\text{cm}^{-1}$, $r \approx 15$ cm and $q \approx 3$, so mode numbers are $n \approx 50$ and

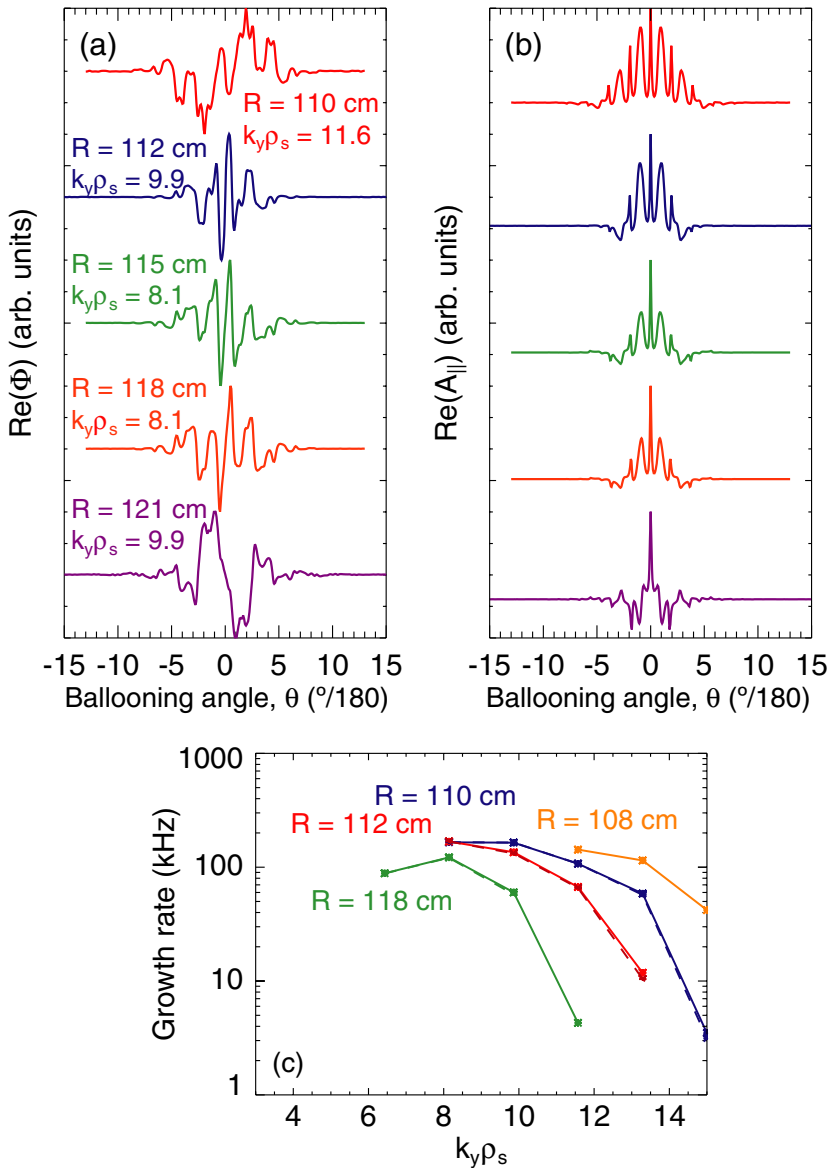

Figure 2. (*a*) and (*b*) $\tilde{\Phi}$ and $\tilde{A}_\parallel$ mode structures for plasma parameters in figure 1 and table 1. (*c*) Growth rate k-spectra for (solid lines) fully electromagnetic simulations and (dashed lines) partially electromagnetic simulations with $\tilde{\Phi}$ and $\tilde{A}_\parallel$.

$m \approx 150$. Conventional microtearing modes exhibit toroidal mode numbers in the range $n \approx 20$–40. From the relation $k_\theta \rho_s = nq(\rho_s/r)$, it is apparent that high-k and conventional microtearing mode numbers can be similar because the high-k microtearing modes are unstable near the magnetic axis, so large $k_\theta \rho_s$ values are counterbalanced by large ρ_s/r values. At larger r, ρ_s decreases and high-k microtearing instabilities at fixed $k_\theta \rho_s$ would likely be stabilized by field line bending characterized by the high-m tearing parameter $\Delta' = -2m/r = -2(k_\theta \rho_s)/\rho_s$ [32].

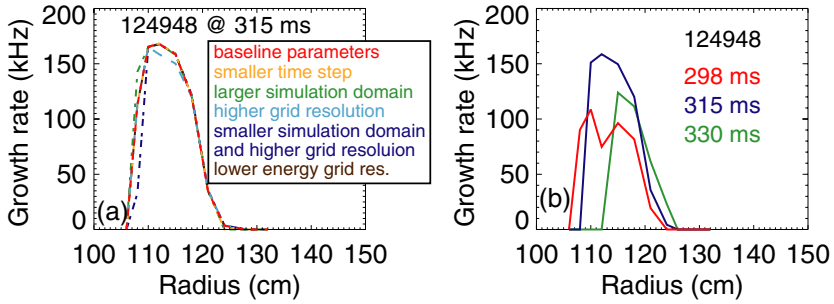

Figure 3. (*a*) Growth rates for the fastest growing microtearing modes from multiple calculations with different simulation parameters based upon plasma parameters in figure 1 at 315 ms. (*b*) Growth rates for the fastest growing microtearing modes based upon plasma parameters at 298, 315 and 330 ms in figure 1.

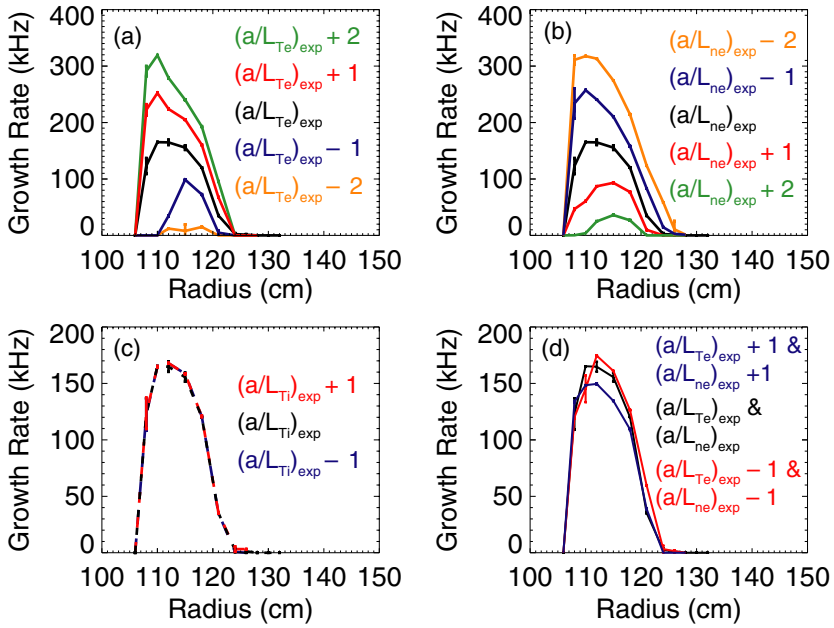

Figure 4. Growth rate dependences on (*a*) electron temperature inverse scale length, (*b*) density inverse scale length, (*c*) ion temperature inverse scale length and (*d*) electron temperature and density inverse scale lengths based upon plasma parameters in figure 1 at 315 ms.

3. Parametric scans

Parametric scans provide additional information about high-k microtearing modes. Figure 4 shows growth rate radial profiles for gradient scale length scans. Growth rate profiles labeled X_{exp} employ measured profile quantities, and profiles labeled $X_{\mathrm{exp}} + Y$ employ measured profile quantities with a uniform shift. The error bars in figure 4 depict the standard deviation of growth rates with three sets of simulation parameters: baseline parameters, finer θ grid ($\Delta\theta = 180^\circ/20$) and larger θ domain ($|\theta| \leqslant 15 \times 180^\circ$). Growth rates increase with higher a/L_{T_e} and decrease with higher a/L_{n_e}, but growth rates are insensitive to a/L_{T_i}. Also, growth

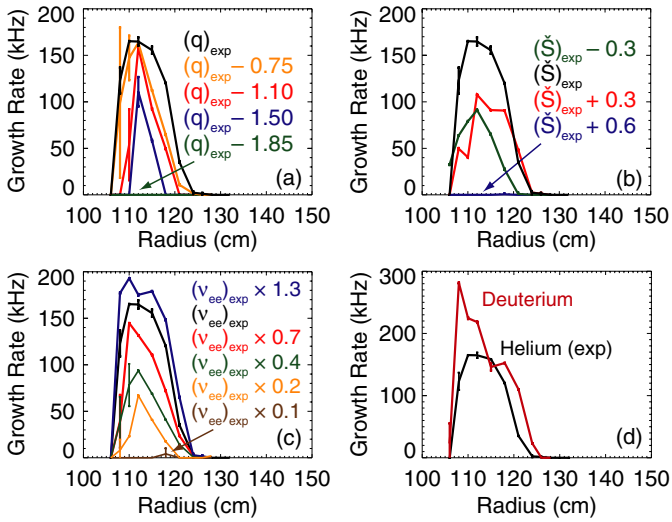

Figure 5. Growth rate dependences on (*a*) safety factor, (*b*) magnetic shear, (*c*) electron–electron collisionality and (*d*) ion species (with fixed electron collisionality) based upon plasma parameters in figure 1 at 315 ms.

rates do not change significantly when a/L_{T_e} and a/L_{n_e} change by the same amount, which suggests $\eta_e \equiv L_{n_e}/L_{T_e}$ is a critical parameter for the mode.

Figures 5(*a*)–(*c*) show growth rate radial profiles for safety factor, magnetic shear and collisionality scans, and figure 5(*d*) shows a comparison between helium and deuterium ion species. Labels and error bars in figure 5 are analogous to labels and error bars in figure 4. Growth rates decrease with lower safety factor (q), and growth rates decrease for higher absolute magnetic shear ($\hat{s}$). Growth rates increase at higher collisionality (ν_{ee}), as expected, because microtearing modes are stable in the collisionless limit [1–3]. Also, growth rates for deuterium ions are higher than growth rates for helium ions with fixed electron collisionality. The higher growth rates for deuterium ions indicate ion dynamics may impact high-k microtearing modes.

4. Microinstabilities across the plasma profile

Previous sections described microtearing modes below the ion gyroscale can be linearly unstable in a NSTX L-mode discharge. In this section, additional unstable modes are investigated. Figures 6(*a*) and (*b*) show growth rate profiles and k-spectra for both microtearing modes with $3 < k_y\rho_s > 15$ and drift-wave modes on the ion gyroscale ('low-k'). Low-k simulations included modes in the range $0.3 < k_y\rho_s < 2.5$, but only modes with $0.8 < k_y\rho_s < 2.1$ were unstable. The unstable low-k modes exhibited even parity $\tilde{\Phi}$ mode structures characteristic of drift-wave turbulence. The low-k modes exhibit growth rates up to 10 kHz and partially overlap radially with high-k microtearing modes. The low-k modes may impact the dynamics of high-k microtearing modes, but only high-k microtearing modes are unstable in the innermost region.

The microtearing modes in figures 2 and 3 exist at wavenumbers comparable to ETG modes. Figures 6(*c*) and (*d*) show growth rate k-spectra and radial profiles for microtearing modes with $3 < k_y\rho_s < 15$ and ETG modes (even parity $\tilde{\Phi}$) with $10 < k_y\rho_s < 30$. Growth

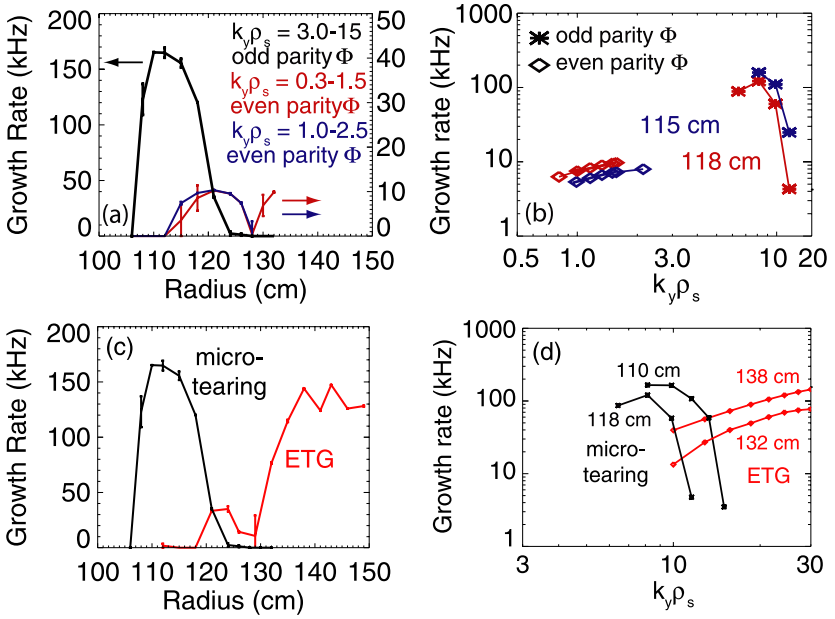

Figure 6. (*a*) Growth rate radial profiles and (*b*) k-spectra for high-k microtearing modes and low-k drift-wave modes. (*c*) Growth rate radial profiles and (*d*) k-spectra for high-k microtearing modes (black) and ETG modes (red).

rates for microtearing and ETG modes are similar, but the modes exist in different radial regions. Specifically, microtearing modes are the most unstable modes near the magnetic axis at $R \lesssim 120\,\mathrm{cm}$, but ETG modes are the most unstable modes in the outer plasma at $R \gtrsim 130\,\mathrm{cm}$. The simulations suggest high-k microtearing modes are more likely to impact transport near the magnetic axis whereas ETG modes are more likely to impact transport in the outer plasma.

5. Summary

Linear GS2 calculations indicate microtearing modes with $3 < k_y\rho_s < 15$ can be linearly unstable in the core region of a NSTX L-mode discharge with HHFW heating. The calculations are converged among simulation parameters, such as time step, and the modes exist throughout an extended radial region near the magnetic axis. The mode structures are narrower in ballooning angle than conventional microtearing modes with $k_y\rho_s \leqslant 1$, but the inferred $k_r\rho_s$ spectra for $\tilde{\Phi}$ extend to $k_r\rho_s$ values comparable to conventional microtearing modes. Mode growth rates increase at higher electron temperature gradient and higher collisionality. In addition, growth rates with deuterium ions are greater than growth rates for helium ions, so ion dynamics may impact the dynamics of high-k microtearing modes. The radial region of high-k microtearing modes partially overlap with low-k drift-wave modes, but the drift-wave modes exhibit smaller growth rates. High-k microtearing modes and ETG modes, however, exist in separate radial regions. Specifically, high-k microtearing modes are the most unstable modes near the magnetic axis, but ETG modes are the most unstable modes in the outer plasma. The high-k microtearing instabilities were studied using a particular NSTX plasma configuration, but a broader survey is needed to assess the ubiquity of the modes in other plasma configurations.

Acknowledgments

This work was supported by the US Department of Energy under Contract Nos DE-FG02-89ER53296, DE-AC02-09CH11466 and DE-SC0001288.

References

[1] Applegate D J *et al* 2007 *Plasma Phys. Control. Fusion* **49** 1113
[2] Roach C M *et al* 2005 *Plasma Phys. Control. Fusion* **47** B323
[3] Applegate D J *et al* 2004 *Phys. Plasmas* **11** 5085
[4] Bourdelle C *et al* 2003 *Phys. Plasmas* **10** 2881
[5] Kotschenreuther M *et al* 2000 *Nucl. Fusion* **40** 677
[6] Rewoldt G, Tang W M, Kaye S and Menard J 1996 *Phys. Plasmas* **3** 1667
[7] Ono M *et al* 2000 *Nucl. Fusion* **40** 557
[8] Ono M *et al* 2001 *Nucl. Fusion* **41** 1435
[9] Kaye S M *et al* 2001 *Phys. Plasmas* **8** 1977
[10] Kaye S M *et al* 2007 *Phys. Rev. Let.* **98** 175002
[11] Kaye S M *et al* 2007 *Nucl. Fusion* **47** 499
[12] Kaye S M, Solomon W, Bell R E, LeBlanc B P, Levinton F M, Menard J E, Rewoldt G, Sabbagh S A, Wang W and Yuh H 2009 *Nucl. Fusion* **49** 045010
[13] Redi M H *et al* 2003 *Proc. 30th EPS Conf. on Controlled Fusion and Plasma Physics* ed R Koch and S Lebedev (Mulhouse: EPS)
[14] Baumgaertel J A, Redi M H, Budny R V, Rewoldt G and Dorland W 2005 *Technical Report* PPPL-4119, Princeton Plasma Physics Laboratory
[15] Levinton F M *et al* 2007 *Phys. Plasmas* **14** 056119
[16] Wong K L *et al* 2007 *Phys. Rev. Lett.* **99** 135003
[17] Wong K L *et al* 2008 *Phys. Plasmas* **15** 056108
[18] Hazeltine R D *et al* 1975 *Phys. Fluids* **18** 1778
[19] Gladd N T *et al* 1980 *Phys. Fluids* **23** 1182
[20] Hassam A B 1980 *Phys. Fluids* **23** 2493
[21] Connor J W *et al* 1990 *Plasma Phys. Control. Fusion* **32** 799
[22] Catto P J and Rosenbluth M N 1981 *Phys. Fluids* **24** 243
[23] Drake J F and Lee Y C 1977 *Phys. Fluids* **20** 1341
[24] Horton W 1999 *Rev. Mod. Phys.* **71** 735
[25] Jenko F *et al* 2000 *Phys. Plasmas* **7** 1904
[26] Dorland W *et al* 2000 *Phys. Rev. Lett.* **85** 5579
[27] Kotschenreuther M, Rewoldt G and Tang W M 1995 *Comput. Phys. Commun.* **88** 128
[28] Hosea J *et al* 2008 *Phys. Plasmas* **15** 056104
[29] Wilson J R *et al* 2003 *Phys. Plasmas* **10** 1733
[30] LeBlanc B P *et al* 2003 *Rev. Sci. Instrum.* **74** 1659
[31] LeBlanc B P 2008 *Rev. Sci. Instrum.* **79** 10E737
[32] Wesson J 2004 *Tokamaks* (Oxford: Oxford University Press)